Dalton Transactions

ROYAL SOCIETY OF CHEMISTRY

PAPER

View Article Online
View Journal | View Issue

Cite this: *Dalton Trans.*, 2022, **51**, 14508

Low-temperature ALD/MLD growth of alucone and zincone thin films from non-pyrophoric precursors†

Anish Philip, ‡[a] Lukas Mai, ‡[b] Ramin Ghiyasi, [a] Anjana Devi *[b] and Maarit Karppinen *[a]

The combined atomic/molecular layer deposition (ALD/MLD) technique is emerging as a state-of-the-art synthesis route for new metal–organic thin-film materials with a multitude of properties by combining those of the inorganic and the organic material. A major part of the studies so far reported have focused on aluminum or zinc alkyls, so-called alucone and zincone films, typically grown from trimethyl aluminum (TMA) or diethyl zinc (DEZ) as the metal-bearing precursor, and a simple aliphatic bi-functional alcohol molecule such as ethylene glycol (EG) as the organic precursor. However, these common precursors possess certain disadvantages: both TMA and DEZ are pyrophoric, DEZ being additionally thermally unstable, while EG has a strong tendency for various unideal reaction modes. Here we report novel ALD/MLD processes for alucone and zincone films based on non-pyrophoric bis-diisopropylamido-[3-(*N*,*N*-dimethylamino)propyl] aluminum(III) [$Al(NiPr_2)_2(DMP)$] and bis-3-(*N*,*N*-dimethylamino)propyl zinc(II) [$Zn(DMP)_2$] precursors in combination with hydroquinone (HQ) as the organic precursor. We demonstrate that the [$Al(NiPr_2)_2(DMP)$] + HQ and [$Zn(DMP)_2$] + HQ ALD/MLD processes work even at record low deposition temperatures (140 °C and 60 °C, respectively) yielding high-quality and relatively stable Al-HQ and Zn-HQ thin films with appreciably high growth rates (2.8 Å / cycle and 3.2 Å / cycle, respectively). Moreover, these ALD/MLD processes are compatible with the corresponding ALD processes, *i.e.* [$Al(NiPr_2)_2(DMP)$] + H_2O and [$Zn(DMP)_2$] + H_2O, for the Al_2O_3 and ZnO films, thus opening up new horizons for the fabrication of novel metal–oxide : organic superlattice structures for *e.g.* flexible gas-barrier coatings or wearable thermoelectrics.

Received 13th July 2022,
Accepted 30th August 2022

DOI: 10.1039/d2dt02279f

rsc.li/dalton

Introduction

Atomic layer deposition (ALD) has been extensively used in industry, especially in microelectronics, as the state-of-the-art gas-phase thin-film fabrication technology, as it offers high-quality conformal inorganic coatings in a highly controllable manner.[1–3] Molecular layer deposition (MLD) is based on the same principles as ALD but for purely organic polymers, while the combination of the two techniques, ALD/MLD, provides an attractive route for the fabrication of intriguing metal–organic thin films for a variety of emerging application fields.[4–8] While the inorganic component in these hybrid materials typically forms the basis for the desired electrical, optical, magnetic or catalytic functionality, the organic component could bring *e.g.* mechanical flexibility,[5,9,10] additional structural/chemical tunability[11–15] or even unforeseen bio- or light-based actions[16–19] for the hybrid material.

Aluminum and zinc are the two prototype metal components most commonly applied in conventional ALD technology; well-established ALD processes developed for these two metals cover a variety of materials ranging from the pure metals[20] and intermetallics[21,22] to metal oxides,[23–26] sulfides,[3,27,28] and nitrides.[29–32] As for the ALD/MLD processes, the Al- and Zn-based metal–organic films deposited so far, include a variety of metal alkyls (so-called alucones/zincones),[33–35] and also carboxylates,[36–38] and amides[39] using organic diols, carboxylic acids or amines, respectively, as the organic precursor. It is well known yet, somewhat surprising, that most of these different Al/Zn-containing thin-film materials have been deposited from the same Al and Zn precursors, *i.e.*, trimethyl aluminum (TMA) and diethyl zinc (DEZ). High volatility and excellent reactivity together with the

[a]*Department of Chemistry and Materials Science, Aalto University, FI-00076 Espoo, Finland. E-mail: anjana.devi@ruhr-uni-bochum.de*
[b]*Inorganic Materials Chemistry, Ruhr University Bochum, 44801 Bochum, Germany. E-mail: maarit.karppinen@aalto.fi*

†Electronic supplementary information (ESI) available. See DOI: https://doi.org/10.1039/d2dt02279f

‡Equal contribution.

commercial availability have made these precursors superiorly popular over the few other aluminum and zinc precursors challenged so far. However, both TMA and DEZ are pyrophoric, which possesses safety issues that complicates the handling of these precursors. Moreover, TMA exists in both monomeric and dimeric forms, and the balance between these two forms affects the precursor volatility and the deposition process itself, making the process less predictable and controllable.[40,41] Additionally, when using TMA for an ALD/MLD process, it is – due to its relatively small size – prone to infiltrate within the growing metal–organic hybrid film, *i.e.* so-called vapor-phase infiltration (VPI).[42]

Aluminum alkoxides of the [Al(OR)$_3$] type have been shown to be promising precursor candidates for ALD of Al_2O_3 films;[43,44] however, among them, the optimal deposition temperature varies strongly depending on the R backbone, being relatively low (around 140 °C) for R = *n*Pr, while significantly high (350–450 °C) for R = Et. For the use of these precursors in ALD/MLD, it is thus important to consider optimal temperature window to match the thermal properties of the organic precursor. Similarly, the increasing thermal instability of DEZ with increasing temperature (starting even at temperatures as low as 60 °C (ref. 45)) should be seriously considered when designing new Zn-based deposition processes. On the other hand, other zinc precursors available have the drawback of high deposition temperature requirement due to the poor volatility and reactivity. Therefore, it is most vital to explore new metal precursors that could enable the deposition of both aluminum and zinc-based hybrid films within the targeted temperature range.

The most common ALD/MLD processes of Al- and Zn-containing hybrid thin films are those that combine the metal component with a bifunctional alcohol.[5,34,35,46,47] Ethylene glycol (EG) served for long as a prototype organic precursor for these depositions.[5,48,49] However, aromatic alcohols have been more recently highlighted as an intriguing option as the π–π interactions between the phenyl groups could stabilize the hybrid structure. In addition to the stability offered by the aromatic rings, higher growth rates have been achieved with the aromatics, which has been attributed to the decreased probability of the unwanted double-surface-reactions to occur with the more rigid aromatic alcohols as compared to their aliphatic counterparts.[36,50,51] Indeed, such double-surface-reactions in case of aliphatic alcohols have been found to reduce the reactive surface sites and thereby to eventually decrease the film growth rate.[50] The superior mechanical properties and improved electrical conductivity are some other reasons for using aromatic alcohols over the aliphatic ones; in particular, hydroquinone (HQ; benzene-1,4-diol) has been considered as a promising option.[9,50–55] From Table 1 listing some representative reported Al-HQ and Zn-HQ processes, the dominating roles of TMA and DEZ as the metal precursor are seen.

Here we present the non-pyrophoric bis-diisopropylamido-[3-(*N*,*N*dimethylamino)propyl] aluminum(III) [Al(NiPr$_2$)$_2$(DMP)][56] and bis-3-(*N*,*N*-dimethylamino)propyl zinc [Zn(DMP)$_2$][57] as highly promising metal precursors for the low temperature deposition of hybrid Al-HQ and Zn-HQ thin films. In our pioneering works, these precursors were shown to work in ALD processes for Al_2O_3 (thermal ALD) and ZnO (plasma-assisted ALD) films. For the former thermal ALD process, the optimal temperature window was 100–180 °C (with a growth rate of 1.0 Å / cycle similar to the common TMA + H_2O processes),[58] while the latter plasma-assisted process worked even at the appreciably low deposition temperature of 60 °C. Here, we demonstrate – firstly – that the [Zn(DMP)$_2$] precursor is reactive enough to yield ZnO films even in combination with water in a conventional thermal ALD process, and then – most importantly – that both [Al(NiPr$_2$)$_2$(DMP)] and [Zn(DMP)$_2$] function well in combination with HQ as the organic precursor in ALD/MLD for the hybrid alucone and zincone films. Very importantly the possibility to use the same metal precursor makes the water-based thermal metal–oxide ALD and the metal–organic ALD/MLD processes mutually combinable, thus opening up new avenues for the low-temperature growth of layer-engineered metal–oxide : organic superlattice

Table 1 Reported ALD/MLD processes for hybrid Al-HQ and Zn-HQ thin films

Inorganic precursor	Deposition temperature (°C)	GPC (Å / cycle)	Material type	Property/application studied	Ref.
TMA	200	6.9	Hybrid	Annealed to graphitic carbon	55
TMA	200	7.0	Hybrid	Annealed to semiconductor	61
TMA	150	7.5	Hybrid	Electrode coating	13
TMA	150	4.1	Hybrid		46
TMA	180	3.5	Hybrid		62
TMA	150	2.2	Hybrid	Electrochemical performance	8
TMA	100	3.4	SL	Barrier properties	67
DEZ	150	2.8	Hybrid	Semiconductor	63
DEZ	220	7.4	SL	Thermoelectrics	64
DEZ	230	4.0	SL	Thermoelectrics	60
DEZ	150	52.3 ng cm^{-2}	Hybrid		9
DEZ	150	2.0	Hybrid	Mechanics, porosity, *etc.*	54
DEZ	200	2.0	Hybrid	Electrical transport	65
DEZ	150	5.4	SL	Porosity & air-degradation	66
DEZ	150	1.6	SL	Thermal conductivity	51
DEZ	150	1.6	Hybrid		53
DEZ	150	2.7	Hybrid		50

(SL) type structures for various advanced applications requiring simultaneously the mechanical flexibility from the organic layers and the specific functional properties of the inorganic layers.[12,23,56,59,60]

Experimental

All the thin films were deposited on 2.0 × 2.0 cm^2 Si(100) substrates in a commercial flow-type hot-wall thermal ALD reactor (F-120 by ASM Ltd); schematics of the reactor with its different temperature zones is shown in Fig. S1, ESI.† The in-house synthesized [Al(NiPr$_2$)$_2$(DMP)] and [Zn(DMP)$_2$] precursor powders were vaporized at 75 and 35 °C, respectively. For the deposition of metal oxide films, deionized water was used as the co-reactant, while in the case of the hybrid metalcone films, the second precursor was hydroquinone (HQ; benzene-1,4-diol) which was routinely vaporized at 90 °C, but we also challenged the ultralow vaporization temperature of 60 °C for it. All the precursors other than deionized water were placed inside the reactor in open boats, while the deionized water cylinder was kept outside the reactor and pulsed at 21 °C. Because of their air sensitivity, the metal precursors were loaded into the precursor boats in a glove box and sealed with paraffin film, which was removed immediately before transferring the precursor boat to the reactor under inert atmosphere. Nitrogen (99.999%; flow rate at 300 SCCM) was used as both the carrier and purge gas between the precursor pulses. The reactor pressure was kept at 3–5 mbar.

All the films were characterized for their thickness, density and roughness with X-ray reflectivity (XRR; PANalytical X'Pert PRO Alfa 1) measurements; the data were fitted using the X'Pert Reflectivity software by PANalytical. For the calculation of the growth-per-cycle (GPC) value, the XRR-determined film thickness value was divided by the number of deposition cycles applied. The XRR pattern fittings were straightforward for both alucone and zincone films, even though there was an uncertainty on the exact molecular formulae of the materials. Therefore, the film densities were also calculated directly from the critical angle (θ_c) values based on the dependency of θ_c on the mean electron density (ρ_e) and mass density (ρ_m) of the film material, using the equation, $\rho_e = (\theta_c^2\pi)/(\lambda^2 r_e)$, where λ is the X-ray wavelength and r_e is the classical electron radius. The mass density was then calculated as $\rho_m = (\rho_e A)/(N_A Z)$, where A is the average molar mass, N_A is the Avogadro constant and Z is the average atomic number. In general, the density values obtained from the XRR pattern fittings and calculations based on the critical angle were in excellent agreement with each other.

The same diffractometer was used to collect the grazing incidence X-ray diffraction (GIXRD) patterns for the films with an incident angle of 0.5°. The chemical (bonding) structure of the films was investigated using Fourier transform infrared (FTIR, Bruker alpha II) spectroscopy analysis. The interference from the silicon substrate was suppressed by subtracting the FTIR spectrum of the bare silicon substrate from the FTIR spectra of the samples.

Results and discussion

We investigated the two metal precursors, [Al(NiPr$_2$)$_2$(DMP)] and [Zn(DMP)$_2$], for both the metal–oxide and metal–organic thin-film fabrication in the low-temperature range of 60–170 °C. The metal–oxide processes were water-based while in the metal–organic processes hydroquinone was used as the organic precursor. One of the advantages of HQ is its relatively low sublimation temperature, which was crucial for the realization of the low-temperature deposition processes. From GIXRD measurements, the resultant Al_2O_3, Al-HQ and Zn-HQ films were amorphous, while the ZnO films were polycrystalline.

[Al(NiPr$_2$)$_2$(DMP)] + HQ process

For the Al-HQ films, the process optimization data are summarized in Fig. 1. This process was investigated within the

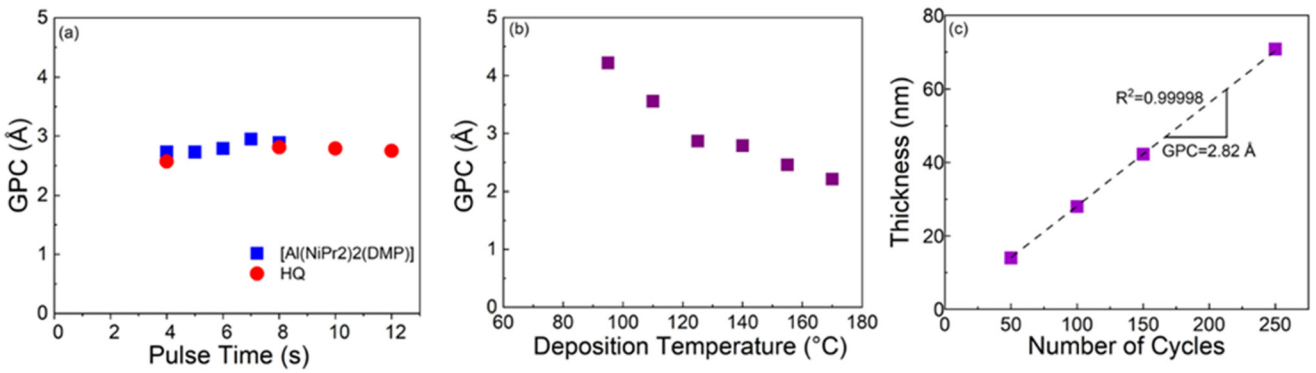

Fig. 1 ALD/MLD process characteristics for the [Al(NiPr$_2$)$_2$(DMP)] + HQ process on Si substrates: (a) saturation curve with individually increased precursor pulse lengths, the other pulse length was fixed at 10 s and 6 s for HQ and [Al(NiPr$_2$)$_2$(DMP)], respectively, (b) GPC *versus* deposition temperature, and (c) linear dependence of film thickness on the number of ALD/MLD cycles applied; in (a) and (c), deposition temperature was 140 °C, in (b) & (c) pulse/purge sequence was: 6 s [Al(NiPr$_2$)$_2$(DMP)]/10 s N_2/8 s HQ/15 s N_2.

temperature range from 95 to 170 °C, the lowest feasible deposition temperature defined by the precursor vaporization temperatures used, *i.e.* 75 °C for [Al(NiPr$_2$)$_2$(DMP)] and 90 °C for HQ. As seen from Fig. 1(b), efficient film growth could be achieved within the entire deposition temperature range investigated; in these temperature-varied experiments the precursor/purge pulsing sequence was: 6 s [Al(NiPr$_2$)$_2$(DMP)]/10 s N$_2$/8 s HQ/15 s N$_2$. It is evident that the GPC value decreases with increasing deposition temperature, from 4.2 Å/cycle at 95 °C to 2.2 Å/cycle at 170 °C. This is a very common trend seen for most of the ALD/MLD processes, and typically explained by the following phenomena (depending on the case): (i) tendency of organic precursors to decompose/desorb at high temperatures, (ii) stickiness of organic molecules at low temperatures towards remaining in the growing film as a kind of reservoir to form additional reaction sites, and (iii) physisorption of metal precursor molecules within the porous metal–organic material at low temperatures.[47,67,68] In principle, the faster film growth at low temperatures could also be caused by precursor condensation, but this seems to be unlikely at least in the present case, taking into account the fact that in the ALD process of [Al(NiPr$_2$)$_2$(DMP)] with water as the co-reactant the inorganic precursor showed no signs of condensation (but rather insufficient reactivity) at low temperatures.[58]

In previous works for the ALD/MLD Al-HQ processes based on TMA as the Al precursor, GPC values ranging from 2.2 to 7.5 Å / cycle at the typical deposition temperatures of 150 and 200 °C have been reported (Table 1). The somewhat lower GPC values obtained here in this temperature range with [Al(NiPr$_2$)$_2$(DMP)] as the aluminum precursor are apparently caused by the more pronounced steric hindrance of the larger ligands in [Al(NiPr$_2$)$_2$(DMP)]. The most important benefit of [Al(NiPr$_2$)$_2$(DMP)] over the TMA is the highly competitive GPC value of 4.2 Å / cycle at 95 °C. Interestingly, this value is higher compared to the value of 3.4 Å / cycle reported for an Al-HQ layer grown from TMA on top of an Al$_2$O$_3$ layer at 100 °C.[69]

To verify the self-limiting growth mode expected for an ideal ALD/MLD process, we confirmed that the GPC value saturated when the precursor pulse lengths of [Al(NiPr$_2$)$_2$(DMP)] and HQ were individually increased; this data is shown in Fig. 1(a). As can be seen, the growth rate is only weakly dependent on the precursor pulse lengths; a small increasing trend is seen for [Al(NiPr$_2$)$_2$(DMP)] up to 7 s, and for HQ up to 8 s. Interestingly, the former pulse length is exactly what was found for the same [Al(NiPr$_2$)$_2$(DMP)] precursor in the water assisted thermal ALD process for the deposition of Al$_2$O$_3$ films.[58] Finally, we demonstrate in Fig. 1(c) that our [Al(NiPr$_2$)$_2$(DMP)] + HQ process obeys the linearity criterion expected for an ALD/MLD process, *i.e.*, that the film thickness increases in a highly linear manner (R^2 = 0.99998) with increasing number of ALD/MLD cycles applied. The GPC value calculated from the data is 2.82 Å / cycle; in these experiments the precursor/purge pulsing sequence was: 6 s [Al(NiPr$_2$)$_2$(DMP)]/10 s N$_2$/8 s HQ/15 s N$_2$, and the deposition temperature was 140 °C.

The film roughness and density values were estimated based on the XRR data fittings (Fig. S2 and S3†). The films were found to be appreciably smooth, the roughness value decreasing from 1.0 to 0.3 nm when the deposition temperature increased from 110 to 155 °C. The obtained film density values increased accordingly from 1.2 to 1.6 g cm^{-3}, being in line with the values previously reported for alucone films. For example, for our Al-HQ film deposited at 140 °C, the density value was exactly the same (1.6 g cm^{-3}) as the value previously reported for an Al-HQ film deposited from TMA at 150 °C.[46]

We investigated the types of chemical species and bonding modes in the Al-HQ films with FTIR spectroscopy; a spectrum recorded for a representative film is displayed in Fig. 2, together with a spectrum for the HQ precursor powder for reference. For HQ, the characteristic ν(O–H) stretching vibration peak is seen at 3160 cm^{-1}, but this is missing in the Al-HQ spectrum indicating that hydroquinone has completely reacted with [Al(NiPr$_2$)$_2$(DMP)] to form the Al–O–C$_6$H$_4$–O–Al units. This is further proven by the appearance of the ν(Al–O) stretching peak at 835 cm^{-1}.[70] Furthermore, only one aromatic ν(C=C) stretching vibration can be found, at 1504 cm^{-1}. The ν(C–O) stretching vibration is detected at 1224 cm^{-1} for the Al-HQ film, *i.e.* at a slightly higher wavenumber compared to the HQ case, as a consequence of the changed binding situation of the oxygen atom. As no characteristic vibrations for amine bonding or aliphatic hydrocarbons are seen, it can be stated, that the reaction of HQ with [Al(NiPr$_2$)$_2$(DMP)] is complete without incorporation of ligand fragments of the amides or the DMP ligand into the thin film. Overall, the Al-HQ spectrum is in good agreement with those seen for other ALD/MLD-grown metal-HQ thin films.[35,46]

Stability of Al-HQ films

Most of the alucone films reported in literature have been unstable in open air. To investigate the stability of our Al-HQ films, we recorded FTIR spectra regularly during their storage

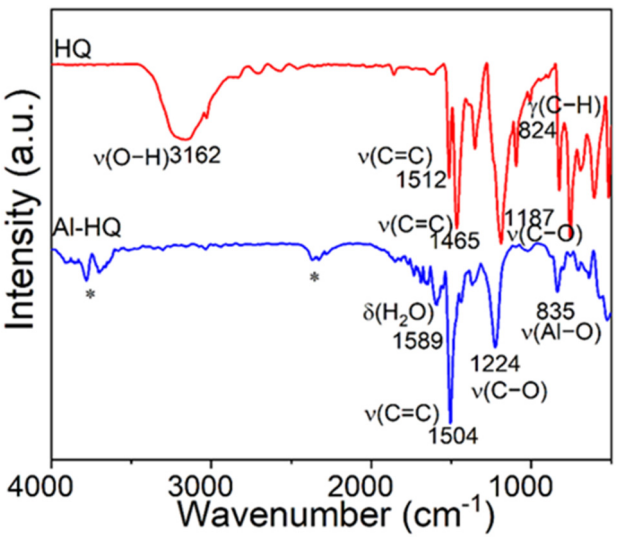

Fig. 2 FTIR spectrum of a 70 nm thick Al-HQ thin film deposited on Si at 140 °C. For comparison the spectrum recorded for the HQ precursor is also shown. The bands marked with * are caused by adsorbed CO$_2$.

under ambient conditions; the spectrum after a two-week storage is displayed in Fig. 3(a) together with a spectrum recorded for the as-deposited film. It can be seen that the same bands as in the as-deposited film can be found for the aged sample, but the band at 1589 cm^{-1} due to the deformation vibration of $\delta(H_2O)$ is more pronounced.[71] Furthermore, in the 3600–4000 cm^{-1} range, a broad band appears, that can be assigned to the ν(O–H) stretch vibrations of water. Unfortunately, this signal is overlapping with the signal of adsorbed CO_2 making a more detailed interpretation difficult. However, we assume that it is most likely caused by water coordinated to the metal center as the organic part still seems to be intact and not affected over time. This observation is in line with the fact that the film thickness was found to decrease during one-day storage in ambient conditions, *e.g.*, for a film deposited with 150 ALD/MLD cycles at 140 °C from 42 to 31 nm. The degree of shrinkage, *i.e. ca.* 25%, observed here for our Al-HQ films deposited from $[Al(NiPr_2)_2(DMP)]$ is of the same order as the values reported by Nilsen *et al.* for their Al-HQ films grown from TMA.[62] Also, the previously reported ethylene glycol based Al-EG films have shown similar deterioration upon exposure to ambient air.[34] While the thickness reduction was somewhat less pronounced (22% after air exposure of 5–6 days), the chemical composition of the Al-EG films changed more dramatically compared to our Al-HQ films, possibly due to the trapping of the smaller EG molecules within the growing Al-EG film leading to subsequent dehydration in addition to the water absorption.

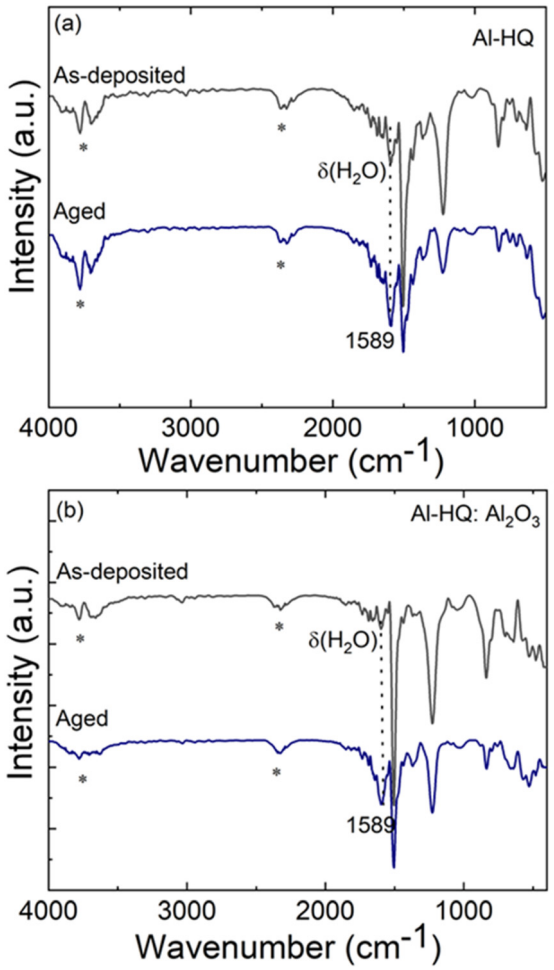

Fig. 3 Stability studies of Al-HQ films: FTIR spectra for (a) a 70 nm thick Al-HQ film immediately after the deposition and aging (two-week) in ambient conditions, and (b) Al-HQ film deposited at 140 °C and capped with 45 nm Al_2O_3 layer measured immediately after the deposition and after one-week storage in ambient conditions. The bands marked with * are caused by adsorbed CO_2.

Because of the instability of the Al-HQ films under ambient conditions, part of the experiments were carried out at the deposition temperature of 140 °C (and not at the lowest temperature of 95 °C), as it allowed us to deposit a capping ALD-Al_2O_3 layer for the Al-HQ films through the $[Al(NiPr_2)_2(DMP)]$ + H_2O process. It is worth mentioning that the ALD-Al_2O_3 process (7 s $[Al(NiPr_2)_2(DMP)]$/10 s N_2/1 s H_2O/30 s N_2) yielded the Al_2O_3 layers with a GPC of 0.72 Å / cycle, in reasonable accordance with our previous report.[58]

We tested the capping layer concept for a 55 nm Al-HQ film (200 cycles) by capping it with an Al_2O_3 layer grown with 250 ALD cycles. Assuming the same GPC value as for bare Al_2O_3 films, this capping layer was estimated to be *ca.* 20 nm thick. However, the resultant total film thickness was found to be 100 nm (instead of the expected thickness of 75 nm), indicating that the growth rate of Al_2O_3 seems to be twice as high on Al-HQ as on Si(100) (such that the obtained Al_2O_3 layer was 45 nm thick). Tentatively we explain this as follows: the Al-HQ film may work as a reservoir for excess water molecules during the H_2O pulse which then reacts with the subsequent $[Al(NiPr_2)_2(DMP)]$ pulse, resulting in additional growth. Interestingly, the reaction of this temporarily incorporated water seems to be complete, as no water vibrations could be detected in the FTIR spectrum immediately after the deposition, see Fig. 3(b). However, after one week storage under ambient conditions, the water vibrations were detected, indicating that the Al_2O_3 capping layer is not completely protecting the Al-HQ film from water absorption. However, it slows down the water diffusion, as for the Al_2O_3-capped Al-HQ the thickness shrinkage was only 10% after one week of storage.

$[Zn(DMP)_2]$ + H_2O and $[Zn(DMP)_2]$ + HQ processes

Similar to the aluminum-based processes, we investigated the low-temperature deposition processes for both Zn-HQ and ZnO films using $[Zn(DMP)_2]$ as the zinc precursor. As $[Zn(DMP)_2]$ could be vaporized at the appreciably low temperature of 35 °C, deposition temperatures as low as 60 °C could be achieved, which is very exciting as there are no reports on low-temperature deposition of hybrid Zn-HQ thin films. Note that for that purpose, we also had to challenge the unusually low evaporation temperature of 60 °C for the HQ precursor. We started the $Zn(DMP)_2$-enabled low-temperature deposition experiments by investigating the feasibility of the ALD growth of ZnO films at 60 °C. From Fig. 4(a), it can be seen that the surface-saturation is reached for $Zn(DMP)_2$ at a pulse length of 10 s (H_2O pulse length at 2 s), yielding a GPC value of

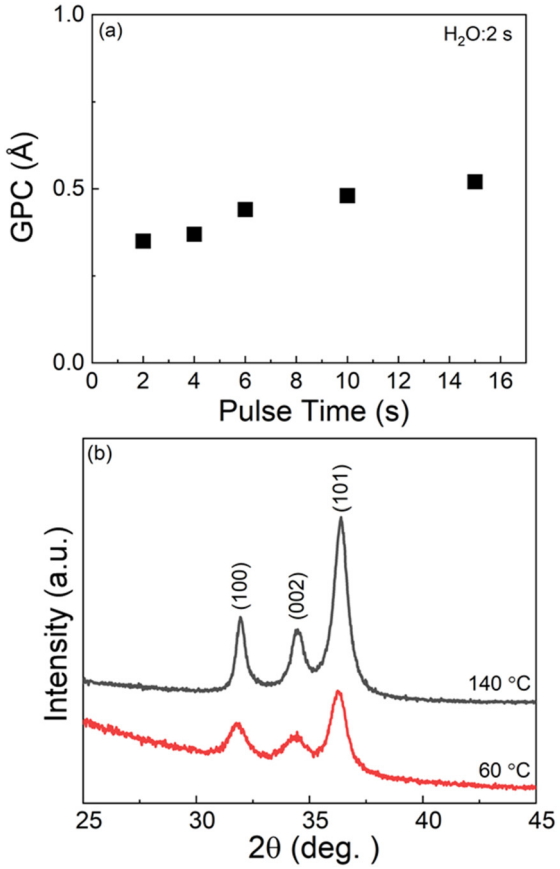

Fig. 4 Confirmation of the feasibility of the low-temperature ALD of ZnO films from $[Zn(DMP)_2]$ and H_2O precursors: (a) saturation study of the $[Zn(DMP)_2]$: the H_2O pulse kept constant at 2 s and the $[Zn(DMP)_2]$ pulse varied; deposition was performed at 60 °C. (b) GIXRD of ZnO deposited on Si(100) at two different temperatures. The total number of cycles was 600 in both cases, the reflections are indexed.

0.49 Å/cycle, which is very similar to the value previously realized in a plasma-enhanced ALD process at the same deposition temperature.[57] The GIXRD patterns shown in Fig. 4(b) for our thermal-ALD ZnO films grown at 60 °C and also at 140 °C for reference, confirm that even the low-temperature deposited ZnO thin film is well crystallized, though the diffraction peak intensities seem to be little lower compared to the film deposited at 140 °C. Here it should be noted that the lower diffraction intensities are explained by the considerably lower thickness of the 60 °C grown film, as both films were deposited with the same number of ALD cycles (600 cycles), yielding more than doubled film thickness for the film deposited at 140 °C (with GPC of 1.1 Å/cycle).

Next, the ALD/MLD process for the Zn-HQ films was investigated in the temperature range from 60 to 250 °C ($[Zn(DMP)_2]$ and HQ were vaporized at temperatures of 35 and 60 °C, respectively), see Fig. 5(b). As expected, the growth rate decreases with increasing deposition temperature, typical to alucones or other zincones.[48] From the precursor saturation curves shown in Fig. 5(a), it is clear that the $[Zn(DMP)_2]$ + HQ process follows the behavior expected for an ALD/MLD process, even at the low deposition temperature of 60 °C. Because of the low deposition temperature, longer than usual purge periods were applied after both precursors to avoid the condensation of the precursors in the film. For $[Zn(DMP)_2]$, the surface saturation is reached with a pulse length of 2 s, whereas HQ requires a considerably longer pulse length of 36 s. This can be explained by the extremely low vapor pressure of HQ at the vaporization temperature used (60 °C, chosen here to enable the low deposition temperatures). As the last confirmation of the ideal ALD/MLD type growth, we show in Fig. 5(c) the linear (R^2 = 0.999) dependence of film thickness on the number of deposition cycles. The GPC value calculated from the data is 3.17 Å / cycle; in these experiments the precursor/purge pulsing sequence was: 2 s $[Zn(DMP)_2]$/15 s N_2/36 s HQ/80 s N_2. The growth rate achieved here is slightly higher than those reported earlier for the DEZ-based processes at 150 °C (Table 1).

The film roughness and density values were estimated based on the XRR data fittings (Fig. S4 and S5†). The density values match very well with the values previously reported for Zn-HQ films. For example, the film deposited at 160 °C showed a density of 1.9 g cm^{-3} (1.8 g cm^{-3} when calculated from critical angle), just like a Zn-HQ film deposited at 150 °C using DEZ as the precursor.[50] Similar density values have been also reported for hybrid films deposited from DEZ and 4-aminophenol.[39] The roughness values of our Zn-HQ films decreased from 3.8 to 0.6 nm, when the deposition temperature increased from 60 to 200 °C respectively.

The FTIR spectrum shown in Fig. 6(a) for our Zn-HQ film deposited at 60 °C, matches well with those previously reported for Zn-HQ films.[63] The absence of vibrations around 3160 cm^{-1} indicates the complete reaction of HQ with $Zn(DMP)_2$. The presence of aromatic ring from HQ is confirmed by the sharp ν(C=C) stretching peak at 1493 cm^{-1}. As in the case of Al-HQ films, the ν(C–O) stretching vibration is shifted to 1211 cm^{-1} from the 1187 cm^{-1} position in HQ. The absence of characteristic aliphatic hydrocarbon or the amine vibrations in the spectrum.

Stability of Zn-HQ films

Compared to their Al-HQ analogues, the Zn-HQ films were found to be more stable. However, during the long-term storage under ambient conditions they also absorb water, as seen from the FTIR spectrum recorded for a Zn-HQ film after a two-weeks storage, see Fig. 6: the broad band around 3200–3500 cm^{-1} corresponds to the ν(O–H) stretching of water and the peak at 1589 cm^{-1} is due to the deformation vibration of water. Importantly, our Zn-HQ films deposited at low temperatures from $Zn(DMP)_2$ are more stable than the previously reported zincone films deposited using DEZ and EG, for which even a one-hour exposure to ambient conditions resulted in the disappearance of the characteristic vibration peaks from the structure and the appearance of water-related peaks,[49] apparently due to quick insertion of water vapor into the ethoxy linkage and simultaneous release of glycol molecules, leading to the complete structure destruction. During an

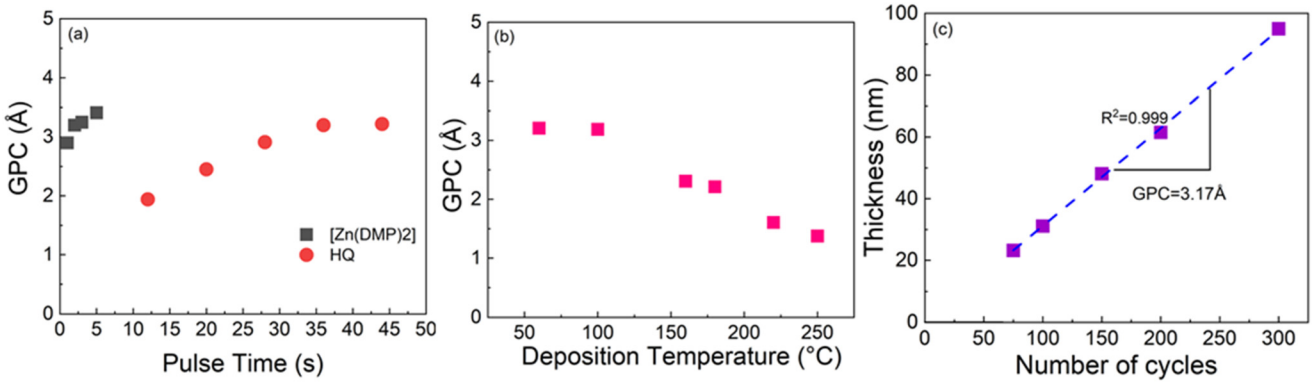

Fig. 5 ALD/MLD characteristics for the [Zn(DMP)$_2$] + HQ process on Si(100): (a) saturation study with individually increased precursor pulse lengths, the other pulse length was fixed at 36 s and 2 s for HQ and [Zn(DMP)$_2$], respectively, (b) GPC *versus* deposition temperature behavior, and (c) linear dependence of film thickness on the number of ALD/MLD cycles applied; in (a) and (c), deposition temperature was 60 °C, in (b) & (c) pulse/purge sequence was: 2 s [Zn(DMP)$_2$]/15 s N_2/36 s HQ/80 s N_2.

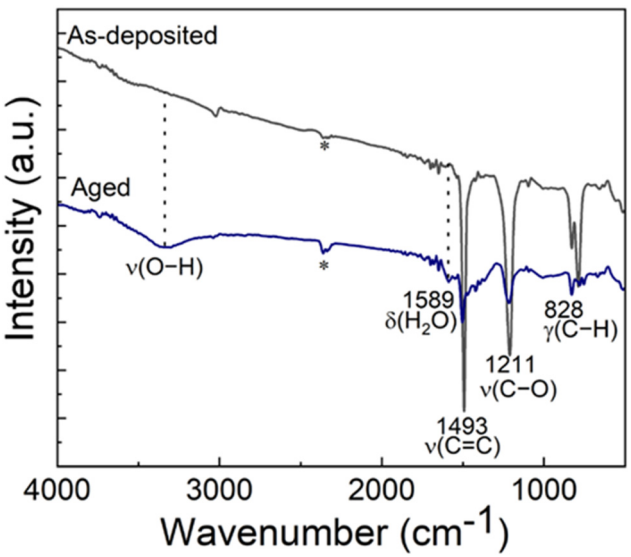

Fig. 6 Stability studies of the Zn-HQ thin films deposited at 60 °C on Si (100) in this study. Comparison of FTIR spectrum of a 95 nm thick Zn-HQ thin film immediately after the deposition and after two weeks in ambient conditions. The bands marked with * are caused by adsorbed CO_2.

extended storage (two weeks) in ambient conditions, the thickness of our Zn-HQ films was found to decrease by 37–45% depending on the initial film thickness. In an earlier study on Zn-HQ films grown using DEZ as the zinc precursor a similar film thickness decrease (by 26%) was seen even after a one day storage in ambient conditions.[51]

Conclusions

This work has demonstrated the possibility to use new non-pyrophoric aluminum and zinc precursors, [Al(NiPr$_2$)$_2$(DMP)] and [Zn(DMP)$_2$], in ALD/MLD in combination with hydroquinone for the growth of alucone (Al-HQ) and zincone (Zn-HQ) thin films at appreciably low temperatures. Both the metal precursors are thermally stable, volatile, and highly reactive and therefore optimal for the low-temperature deposition of new metal–organic thin films. Hydroquinone, on the other hand, is a well-known MLD precursor with sufficiently high vapor pressure, even at the record low vaporization temperature of 60 °C as used here. The processes were shown to fulfil all the typical criteria of ideal ALD/MLD type self-saturated layer-by-layer film growth characteristics.

Like the alucone and zincone films fabricated from other precursors, our Al-HQ and Zn-HQ films grown from [Al(NiPr$_2$)$_2$(DMP)] and [Zn(DMP)$_2$] were not fully stable under ambient conditions, especially upon long term storage. However, our Zn-HQ films deposited at low temperatures from [Zn(DMP)$_2$] were found to be more stable than the previously reported zincone films deposited using DEZ. For the Al-HQ films, we demonstrated the possibility to tackle the instability issue by depositing a thin gas-barrier Al_2O_3 layer from the same Al(NiPr$_2$)$_2$(DMP) precursor and under similar deposition conditions.

Finally, we like to emphasize the future potential in now having both the water-assisted thermal ALD processes for the Al_2O_3 and ZnO films and the ALD/MLD processes for the hybrid AL-HQ and Zn-HQ films, based on the same metal precursors and working in the same low deposition temperature range, for combining these processes for various layer-engineered multilayer structures. One of the apparent application fields of such multilayer structures would be in ZnO-based thermoelectric coatings in particular on flexible (temperature sensitive) substrates, in which Al-doping could be applied to increase the carrier concentration and hydroquinone layers could be inserted to create inorganic/organic interfaces to block the phonon conduction.[59,72]

Conflicts of interest

There are no conflicts of interest to declare.

Author contributions

The manuscript was written through contributions of all authors.

Acknowledgements

We acknowledge the funding from Academy of Finland (Profi 3), and the use of the RawMatTERS Finland Infrastructure (RAMI) at Aalto University. The authors at RUB thank the Deutsche Forschungsgemeinschaft (DFG) for the funding within the DFG-SFB-TR-87 Collaborative Research Centre. Also, the mobility project ALPMOH, funded by DAAD and Academy of Finland is gratefully acknowledged.

References

1 R. W. Johnson, A. Hultqvist and S. F. Bent, *Mater. Today*, 2014, **17**, 236–246.
2 S. M. George, *Chem. Rev.*, 2010, **110**, 111–131.
3 T. Suntola, *Mater. Sci. Rep.*, 1989, **4**, 261–312.
4 J. Multia and M. Karppinen, *Adv. Mater. Interfaces*, 2022, **9**, 2200210.
5 X. Meng, *J. Mater. Chem. A*, 2017, **5**, 18326–18378.
6 H. Zhou and S. F. Bent, *J. Vac. Sci. Technol., A*, 2013, **31**, 040801.
7 S. M. George, B. Yoon and A. A. Dameron, *Acc. Chem. Res.*, 2009, **42**, 498–508.
8 Z. Chen, H. Wang, X. Wang, P. Chen, Y. Liu, H. Zhao, Y. Zhao and Y. Duan, *Sci. Rep.*, 2017, **7**, 40061.
9 B. Yoon, Y. Lee, A. Derk, C. B. Musgrave and S. M. George, *ECS Trans.*, 2011, **33**, 191–195.
10 A. Philip, J. P. Niemelä, G. C. Tewari, B. Putz, T. E. J. Edwards, M. Itoh, I. Utke and M. Karppinen, *ACS Appl. Mater. Interfaces*, 2020, **12**, 21912–21921.
11 O. Lidor-shalev, N. Leifer, M. Ejgenberg, H. Aviv, I. Perelshtein, G. Goobes, M. Noked and Rosy, *Batter. Supercaps Artic.*, 2021, **4**, 1739–1748.
12 T. Tynell, A. Giri, J. Gaskins, P. E. Hopkins, P. Mele, K. Miyazaki and M. Karppinen, *J. Mater. Chem. A*, 2014, **2**, 12150–12152.
13 D. Molina Piper, Y. Lee, S. B. Son, T. Evans, F. Lin, D. Nordlund, X. Xiao, S. M. George, S. H. Lee and C. Ban, *Nano Energy*, 2016, **22**, 202–210.
14 J. P. Niemelä and M. Karppinen, *Dalton Trans.*, 2015, **44**, 591–597.
15 X. Li, A. Lushington, J. Liu, R. Li and X. Sun, *Chem. Commun.*, 2014, **50**, 9757–9760.
16 A. Philip, Y. Zhou, G. C. Tewari, S. van Dijken and M. Karppinen, *J. Mater. Chem. C*, 2022, **10**, 294–300.
17 M. Rogowska, P. A. Hansen, H. H. Sønsteby, J. Dziadkowiec, H. Valen and O. Nilsen, *Dalton Trans.*, 2021, **50**, 12896–12905.
18 K. B. Lausund, M. S. Olsen, P. A. Hansen, H. Valen and O. Nilsen, *J. Mater. Chem. A*, 2020, **8**, 2539–2548.
19 A. Khayyami, A. Philip and M. Karppinen, *Angew. Chem., Int. Ed.*, 2019, **58**, 13400–13404.
20 Y. J. Lee and S. W. Kang, *Electrochem. Solid-State Lett.*, 2002, **5**, C91–C93.
21 J. Xiang, Y. Ding, L. Du, C. Xu, T. Li, X. Wang, J. Li and C. Zhao, *ECS J. Solid State Sci. Technol.*, 2016, **5**, P299–P303.
22 R. Ghiyasi, A. Philip, J. Liu, J. Julin, T. Sajavaara, M. Nolan and M. Karppinen, *Chem. Mater.*, 2022, **34**, 5241–5248.
23 T. Tynell and M. Karppinen, *Semicond. Sci. Technol.*, 2014, **29**, 043001.
24 S. O'Brien, M. G. Nolan, M. Çopuroglu, J. A. Hamilton, I. Povey, L. Pereira, R. Martins, E. Fortunato and M. Pemble, *Thin Solid Films*, 2010, **518**, 4515–4519.
25 G. Marin, R. Funahashi and M. Karppinen, *Adv. Eng. Mater.*, 2020, **22**, 2000535.
26 M. D. Groner, J. W. Elam, F. H. Fabreguette and S. M. George, *Thin Solid Films*, 2002, **413**, 186–197.
27 S. Sinha, N. Mahuli and S. K. Sarkar, *J. Vac. Sci. Technol., A*, 2015, **33**, 01A139.
28 J. Kuhs, Z. Hens and C. Detavernier, *J. Vac. Sci. Technol., A*, 2018, **36**, 01A113.
29 S. Sinha and S. K. Sarkar, *RSC Adv.*, 2014, **4**, 47177–47183.
30 D. Riihelä, M. Ritala, R. Matero, M. Leskelä, J. Jokinen and P. Haussalo, *Chem. Vap. Deposition*, 1996, **2**, 277–283.
31 R. G. Parkhomenko, O. De Luca, Ł. Kołodziejczyk, E. Modin, P. Rudolf, D. M. Martínez, L. Cunha and M. Knez, *Dalton Trans.*, 2021, **50**, 15062–15070.
32 M. G. Ambartsumov, V. A. Tarala, M. S. Nikova, S. O. Krandievsky and L. V. Kozhitov, *Surf. Interfaces*, 2021, **27**, 101559.
33 M. Vähä-Nissi, P. Sundberg, E. Kauppi, T. Hirvikorpi, J. Sievänen, A. Sood, M. Karppinen and A. Harlin, *Thin Solid Films*, 2012, **520**, 6780–6785.
34 A. A. Dameron, D. Seghete, B. B. Burton, S. D. Davidson, A. S. Cavanagh, J. A. Bertrand and S. M. George, *Chem. Mater.*, 2008, **20**, 3315–3326.
35 B. Yoon, B. H. Lee and S. M. George, *J. Phys. Chem. C*, 2012, **116**, 24784–24791.
36 P. Sundberg and M. Karppinen, *Beilstein J. Nanotechnol.*, 2014, **5**, 1104–1136.
37 K. B. Klepper, O. Nilsen and H. Fjellvåg, *Dalton Trans.*, 2010, **39**, 11628–11635.
38 A. Khayyami and M. Karppinen, *Chem. Mater.*, 2018, **30**, 5904–5911.
39 A. Sood, P. Sundberg and M. Karppinen, *Dalton Trans.*, 2013, **42**, 3869–3875.
40 J. P. Mccullough, J. F. Messerly, R. T. Moore and S. S. Todd, *J. Phys. Chem.*, 1963, **67**, 677–679.
41 R. L. Puurunen, *Appl. Surf. Sci.*, 2005, **245**, 6–10.
42 I. Azpitarte, G. A. Botta, C. Tollan and M. Knez, *RSC Adv.*, 2020, **10**, 15976–15982.
43 L. Hiltunen, H. Kattelus, M. Leskelä, M. Mäkelä, L. Niinistö, E. Nykänen, P. Soininen and M. Tiitta, *Mater. Chem. Phys.*, 1991, **28**, 379–388.

44 F. S. M. Hashemi, L. Cao, F. Mattelaer, T. Sajavaara, J. R. van Ommen and C. Detavernier, *J. Vac. Sci. Technol., A*, 2019, **37**, 040901.
45 T. Muneshwar, G. Shoute, D. Barlage and K. Cadien, *J. Vac. Sci. Technol., A*, 2016, **34**, 050605.
46 D. Choudhury, S. K. Sarkar and N. Mahuli, *J. Vac. Sci. Technol., A*, 2015, **33**, 01A115.
47 B. H. Lee, B. Yoon, A. I. Abdulagatov, R. A. Hall and S. M. George, *Adv. Funct. Mater.*, 2013, **23**, 532–546.
48 B. Yoon, J. L. O'Patchen, D. Seghete, A. S. Cavanagh and S. M. George, *Chem. Vap. Deposition*, 2009, **15**, 112–121.
49 Q. Peng, B. Gong, R. M. VanGundy and G. N. Parsons, *Chem. Mater.*, 2009, **21**, 820–830.
50 J. Liu, B. Yoon, E. Kuhlmann, M. Tian, J. Zhu, S. M. George, Y. C. Lee and R. Yang, *Nano Lett.*, 2013, **13**, 5594–5599.
51 M. Aghaee, J. P. Niemelä, W. M. M. Kessels and M. Creatore, *Dalton Trans.*, 2019, **48**, 3496–3505.
52 J. W. Dumont and S. M. George, *J. Phys. Chem. C*, 2015, **119**, 14603–14612.
53 D. Choudhury, G. Rajaraman and S. K. Sarkar, *RSC Adv.*, 2015, **5**, 29947–29952.
54 S. H. Song, S. T. Hwang and B. H. Choi, *Thin Solid Films*, 2020, **706**, 138082.
55 S. Lee, H. M. Kim, G. H. Baek and J. S. Park, *ACS Appl. Mater. Interfaces*, 2021, **13**, 60144–60153.
56 L. Mai, N. Boysen, D. Zanders, T. de los Arcos, F. Mitschker, B. Mallick, G. Grundmeier, P. Awakowicz and A. Devi, *Chem. – Eur. J.*, 2019, **25**, 7489–7500.
57 L. Mai, F. Mitschker, C. Bock, A. Niesen, E. Ciftyurek, D. Rogalla, J. Mickler, M. Erig, Z. Li, P. Awakowicz, K. Schierbaum and A. Devi, *Small*, 2020, **16**, 1907506.
58 L. Mai, M. Gebhard, T. de los Arcos, I. Giner, F. Mitschker, M. Winter, H. Parala, P. Awakowicz, G. Grundmeier and A. Devi, *Chem. – Eur. J.*, 2017, **23**, 10768–10772.
59 T. Tynell, I. Terasaki, H. Yamauchi and M. Karppinen, *J. Mater. Chem. A*, 2013, **1**, 13619–13624.
60 F. Krahl, A. Giri, J. A. Tomko, T. Tynell, P. E. Hopkins and M. Karppinen, *Adv. Mater. Interfaces*, 2018, **5**, 1701692.
61 S. Lee, G. H. Baek, J. H. Lee, D. W. Choi, B. Shong and J. S. Park, *Appl. Surf. Sci.*, 2018, **458**, 864–871.
62 O. Nilsen, K. B. Klepper, H. Ø. Nielsen and H. Fjellvåg, *ECS Trans.*, 2008, **16**, 3–14.
63 J. Huang, H. Zhang, A. Lucero, L. Cheng, S. KC, J. Wang, J. Hsu, K. Cho and J. Kim, *J. Mater. Chem. C*, 2016, **4**, 2382–2389.
64 R. Ghiyasi, G. C. Tewari and M. Karppinen, *J. Phys. Chem. C*, 2020, **124**, 13765–13770.
65 C. Liu, J.-B. Fang, Y.-Q. Cao, D. Wu and A.-D. Li, *Appl. Phys. Lett.*, 2020, **117**, 031601.
66 J. Huang, A. T. Lucero, L. Cheng, H. J. Hwang, M.-W. Ha and J. Kim, *Appl. Phys. Lett.*, 2015, **106**, 123101.
67 J. Multia, J. Heiska, A. Khayyami and M. Karppinen, *ACS Appl. Mater. Interfaces*, 2020, **12**, 41557–41566.
68 N. M. Adamczyk, A. A. Dameron and S. M. George, *Langmuir*, 2008, **24**, 2081–2089.
69 J. Han, T. Kim, D. Kim, H. L. Yang and J. Park, *Dalton Trans.*, 2021, **50**, 15841–15848.
70 G. L. Fisher, A. V. Walker, A. E. Hooper, T. B. Tighe, K. B. Bahnck, H. T. Skriba, M. D. Reinard, B. C. Haynie, R. L. Opila, N. Winograd and D. L. Allara, *J. Am. Chem. Soc.*, 2002, **124**, 5528–5541.
71 J.-J. Max and C. Chapados, *J. Chem. Phys.*, 2009, **131**, 184505.
72 G. Luka, L. Wachnicki, B. S. Witkowski, R. Jakiela and I. S. Virt, *Mater. Des.*, 2017, **119**, 297–302.